

# NUMERICAL ANALYSIS OF THE BEHAVIOUR OF NOTCHED SPECIMENS AT VARIOUS TESTING TEMPERATURES USING AN ELASTIC DAMAGE MODEL

S. DJAKNOUN<sup>1,2\*</sup>, E. OUEDRAOGO<sup>1</sup> and A. AHMED BENYAHIA<sup>2</sup>

<sup>1</sup> Grenoble INP, UJF, CNRS  
Laboratoire 3SR, UMR 5521,  
Domaine Universitaire, BP 53, 38041 GRENOBLE cedex 09, FRANCE  
E-mail: Samira.Djaknoun@hmg.inpg.fr, Evariste.Ouedraogo@grenoble-inp.fr

<sup>2</sup> Université des Sciences et de la Technologie Houari Boumedienne (USTHB)  
Laboratoire de Mécanique Avancée, FGM&GP de L'USTHB  
BP 32 El-Alia, 1611 Alger, ALGERIA.  
Email: sdjaknoun@usthb.dz, aahmedbenyahia@usthb.dz

**Key words:** Numerical modelling, three-point bending tests, notched specimens, damage, stress analysis.

**Abstract:** The study described in this paper was based on some recently published results of research on the behaviour of high-performance concrete in three-point bending tests carried out on notched specimens at various testing temperatures. In this study, the trends in the stress intensity factor and the fracture energy of the concrete with increasing testing temperature were determined. Numerical modelling of three-point bending tests was conducted to examine the formation of damage and the related stress fields. The analysis is based on elasticity coupled with Mazars' damage model for non-local conditions. The numerical model was meshed with both triangular and quadrangular quadratic finite elements. The mesh was refined with triangular elements in the central zone around the vicinity of the notch plane. The model was run for plane stress conditions. The focus of this study was on the analysis of changes in stresses and damage fields with increasing temperature. The numerical modelling clearly showed that the major stress, strain and damage were located in the vicinity of the notch plane. A detailed analysis is presented of the stress components along some nodes located in the notch plane. The results of this study illustrate the complexity of normal and shear stress fields and the consistency of the modelling.

## 1. INTRODUCTION

In recent research, high-performance concrete was studied at elevated temperatures in three-point bending tests of notched specimens. Trends in material durability parameters such as the stress intensity factor  $K_{IC}$  and the fracture energy  $G_F$  with increasing temperature were determined [1]. The localisation of stress in the notch plane raises questions about the stress and strain distribution in the vicinity of the notch plane, and the stress distribution should be checked for consistency with mode I fracture.

The three-point bending tests of high-performance concrete conducted in recent research [1] have also been modelled numerically. The focus of the study described in this paper is on the evolution of stress and damage in high-performance concrete, especially along the notch plane where the deformation is localised. The modelling was based on elasticity coupled with Mazars' scalar isotropic damage model [2, 3]. The distributions of stress and damage and the evolution of stresses in the most constrained zones with increasing loading are discussed in this paper.

## 2. NUMERICAL MODELLING OF THE THREE-POINT BENDING TEST

### 2.1 Boundary conditions

The type of specimen used in the experimental tests was modelled as a beam of high-performance concrete measuring 160 mm in length, with a square cross section of 25 mm on a side and a 10-mm notch length. The beam was modelled as supported at two points 120 mm

apart. To simulate the loading applied to the tested beams, a displacement is imposed at the centre of the top face of the beam. Plane stress conditions in the x (longitudinal) and y (transverse) directions were assumed. The whole beam was modelled because it was anticipated that some of the stresses or the damage field could evolve asymmetrically. The choice was made not to impose symmetry boundary conditions (to reduce the number of nodes) that could have influenced the solution (Fig. 1).

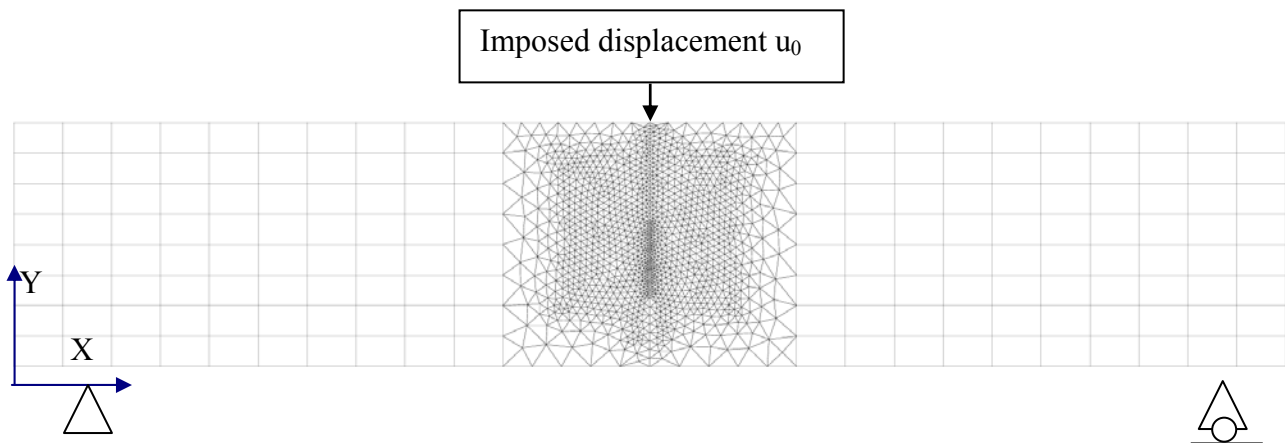


Fig. 1. Mesh of the model with different boundary and loading conditions. Due to the presence of the narrow notch, two mesh areas (coarse and fine) were constructed to optimise the calculations.

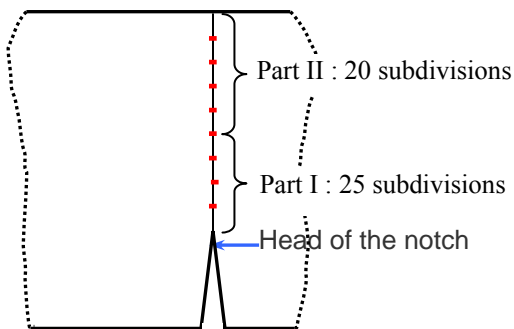


Fig. 2. Discretisation of the resistant ligament: future research will address the nodes located in this ligament.

### 2.2 Model meshing

Because the stress and damage will exhibit strong gradients in the median plane on the one hand and because the thickness of the cut is only 0.2 mm on the other hand, it is essential that the mesh near the median plane and around the crack be very fine, i.e., approximately the thickness of the crack. In contrast, for areas located far from

the median plane, a coarser mesh is sufficient and also has the advantage of minimising the number of finite elements and reducing the computation time. To address these requirements, the mesh was constructed in parts: a central, dense area gradually approaching the notch plane, meshed using quadratic triangular elements; and two parts located on either side of the central area, meshed using quadratic quadrangular elements. The fineness of the mesh along the notch plane was driven by adjusting the number of subdivisions of the line from the crack tip to the upper surface of the specimen, a length of 15 mm for a specimen with a notch length  $a_0$  of 10 mm. The subdivisions are illustrated in Fig. 2. Part I, which is 5 mm long, is divided into 25 parts, and part II, which is 10 mm long, is divided into 20 parts. Future research will focus on the nodes belonging to this ligament. The nonlinear calculations were run using the CAST3M finite element code.

### 3. CONSTITUTIVE EQUATIONS AND MODEL IDENTIFICATION

#### 3.1 Mazars' damage model

The numerical model used in this study was based on elastic behaviour coupled with an isotropic damage model driven by a single scalar parameter  $D$ . The concept of equivalent strain was introduced to characterize the local extension of the material. According to the damage model, damage occurs when the deformation reaches a certain threshold  $K$ . The damage occurrence criterion is expressed as follows:

$$f(\varepsilon, K) = \tilde{\varepsilon} - K(D) = 0 \quad (1)$$

where  $K$  is a function that represents the damage threshold:  $K = K(D) = \varepsilon_{D0}$

This is the limit strain in a uniaxial tension test above which damage can occur in the material.

The form proposed by Mazars for  $\tilde{\varepsilon}$  is the following:

$$\tilde{\varepsilon} = \sqrt{(\langle \varepsilon_1 \rangle_+)^2 + (\langle \varepsilon_2 \rangle_+)^2 + (\langle \varepsilon_3 \rangle_+)^2} \quad (2)$$

where  $\varepsilon_i$  are the three principal strains and  $\langle \varepsilon_i \rangle_+$  are defined as follows:

$$\begin{aligned} \langle \varepsilon_i \rangle_+ &= \varepsilon_i & \varepsilon_i &\geq 0 \\ \langle \varepsilon_i \rangle_+ &= 0 & \varepsilon_i &\leq 0 \end{aligned} \quad (3)$$

The equivalent strain takes into account only the positive value of the principal strain, which is to say, the tensile strain. However, tensile strain can be induced by tensile stress but also by compressive stress. The damage parameters related to these distinct states of stress are  $D_T$  and  $D_C$  for tensile and compressive states of stress, respectively. The damage  $D$  occurring in the material is a function of the contributions of  $D_T$  and  $D_C$  and is expressed as follows:

$$D = \alpha_T \cdot D_T + (1 - \alpha_T) \cdot D_C \quad (4)$$

where:

$$\alpha_T = \sum_i \frac{H_i \varepsilon_{Ti} (\varepsilon_{Ti} + \varepsilon_{Ci})}{\tilde{\varepsilon}^2} \quad (5)$$

with

$$\begin{aligned} H_i &= 0 & \text{Si } \varepsilon_i &< 0 \\ H_i &= 1 & \text{Si } \varepsilon_i &> 0 \end{aligned} \quad (6)$$

The parameters  $D_T$  and  $D_C$  are explicitly related to the equivalent strain and the strain threshold, as shown in the following equations:

$$D_T = 1 - \frac{\varepsilon_{D0}(1 - A_T)}{\tilde{\varepsilon}_M} - \frac{A_T}{\exp[B_T(\tilde{\varepsilon}_M - \varepsilon_{D0})]} \quad (7)$$

$$D_C = 1 - \frac{\varepsilon_{D0}(1 - A_C)}{\tilde{\varepsilon}_M} - \frac{A_C}{\exp[B_C(\tilde{\varepsilon}_M - \varepsilon_{D0})]} \quad (8)$$

where  $\tilde{\varepsilon}_M$  is the maximum equivalent strain and  $\varepsilon_{D0}$  is the damage threshold. The coefficients  $A$  ( $A_C$  and  $A_T$ ) and  $B$  ( $B_T$  and  $B_C$ ) are the material tensile and compressive damage parameters that are to be determined theoretically in uniaxial monotonic loading in tension and compression tests, respectively. Under these conditions, the expression of the model in a uniaxial loading path is as follows:

$$\sigma = \varepsilon_M E_0 (1 - D(\varepsilon_M)) \quad (9)$$

The original feature of this model is the use of a distortion criterion imposed by introducing the concept of equivalent strain. In summary, the values of the six parameters  $E_0$ ,  $\varepsilon_{D0}$ ,  $A_T$ ,  $B_T$ ,  $A_C$  and  $B_C$  are to be determined.

#### 3.2 Identification of the model

Mazars' model has six parameters whose values need to be determined to conduct numerical modelling. These parameter values can be determined theoretically from uniaxial tension and uniaxial compression tests. However, stable and reliable uniaxial tensile tests are difficult to conduct even at room temperature. Special tests such as the STAND test (to identify diffuse damage) have been developed, but they are quite complex to implement and difficult to conduct at high temperatures. Uniaxial compression tests are easier to perform at high temperatures. In this study, we relied in part on results obtained by Mohsen Roosefid (2006) [4], who employed the Mazars model at various temperatures on the basis of uniaxial compression and three-point bending tests of refractory concretes for conditions comparable to those of our study. From the initial damage parameter sets obtained

for a given temperature, we succeeded, by successive variation of these parameters, in reproducing the force–displacement behaviour of the material exhibited in the three-point bending tests. The identification is conducted at a given testing temperature using isothermal test results. The identification procedure is long and tedious, and is not, in our view, of real interest to the reader, so it is not presented in this paper. The calculations run to identify the parameter values were performed assuming a non-local application of the Mazars model and a characteristic length  $l_c$  of 5 mm.

In the identification process of the model parameters, none of the parameter values was fixed a priori. The process essentially consisted of trying to obtain the best fit between the overall experimental curves obtained and the modelled curves. Fig. 3 shows that the modelled curves match the experimental curves well for up to 50 to 70% of the total loading. In the post-peak domain corresponding to softening behaviour, the modelled curves tend to differ notably from the experimental curves.

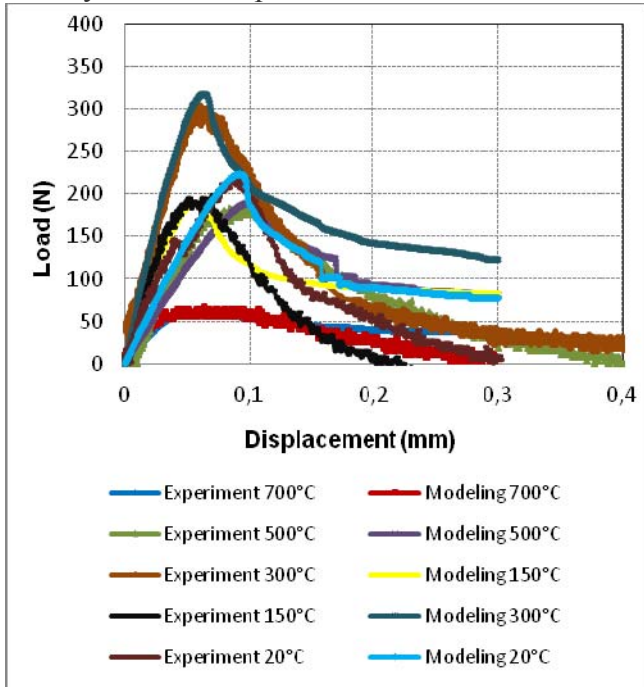


Fig. 3. Modelling of the material response in three-point bending tests at various temperatures with the best retained parameters of Mazars’ model after the identification process.

In summary, it is likely that the damage model used is inapplicable to post-peak

behaviour. We believe, however, that the Mazars prediction model is satisfactory and convenient for use in investigating stress and damage distributions in notched specimens.

## 4. RESULTS AND DISCUSSION

### 4.1 Stress distributions

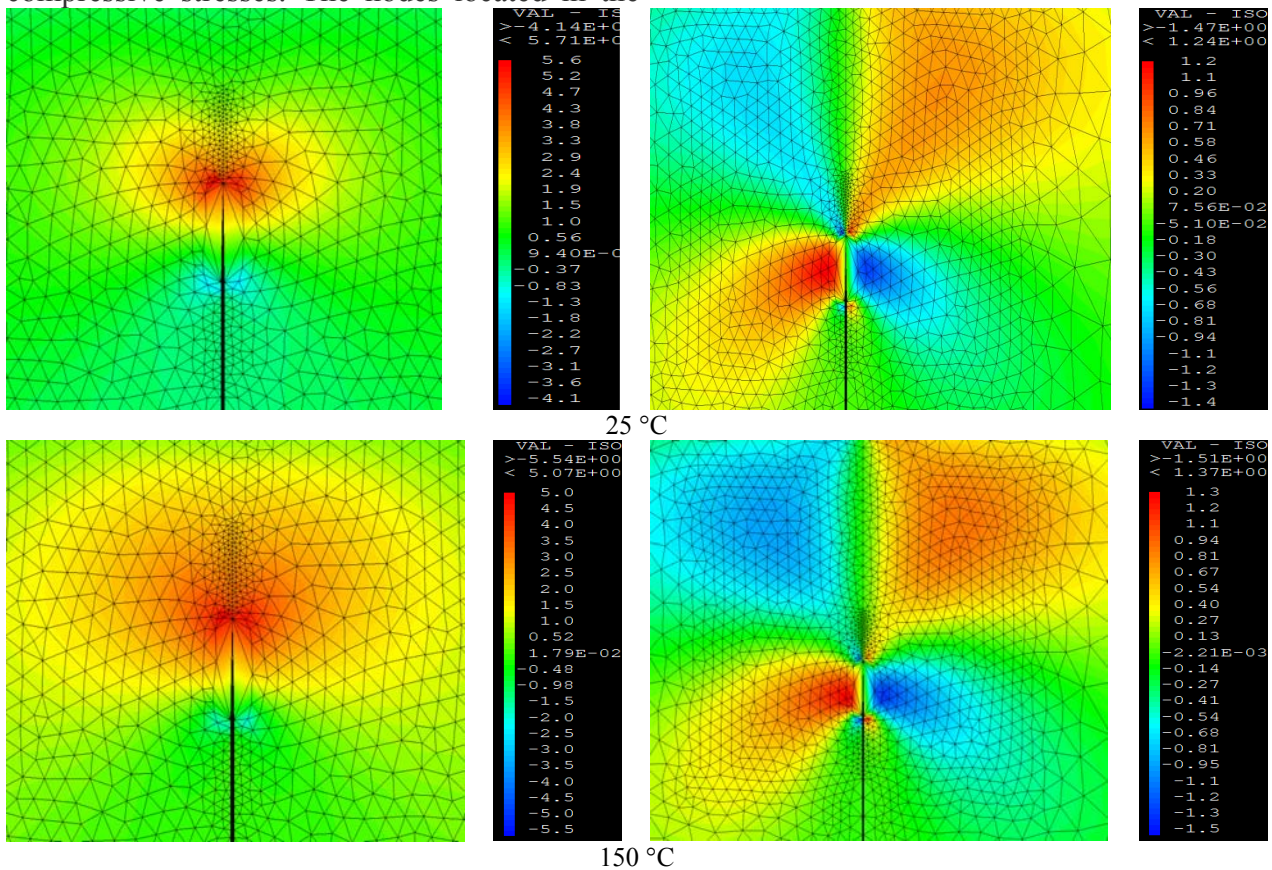
The distribution of the normal  $\sigma_{XX}$  and shear  $\sigma_{XY}$  stresses at the end of the loading ( $u_0=0.3$  mm) are displayed in Fig. 4, on the left and right sides, respectively. It is striking to observe that the stress state is very particular in the central area surrounding the notch plane of the specimen. Of course, a neutral axis separates the section into two parts: an upper part in compression and a lower part in tension. However, while the simple bending of an unnotched beam would have a nearly uniaxial stress state ( $\sigma_{XX} \neq 0$  et  $\sigma_{YY} = \sigma_{ZZ} = 0$ ) in the median plane of the beam, the state of stress in a notched beam is more complex and closer to a state of biaxial tension in the low zone near the crack tip. The principal stresses  $\sigma_{XX}$  (Fig. 4) and  $\sigma_{YY}$  (not displayed here) are positive (tension) and comparable in magnitude in the tension zone around the notch plane. In general, all the  $\sigma_{XX}$  and  $\sigma_{YY}$  maps indicate a logical area of stress concentration around the crack tip that is a singular point of the specimen. Strain localisation around the notch plane observed during the bending test induces a localisation of the stresses that is evident in the maps.

The maximum shear stress shown on the right side of Fig. 4 is reached near the crack tip and at particular zones all around the crack tip at a distance of 5 to 7 finite elements, which is equivalent to 1 to 1.5 mm. The maximum shear stress is approximately 1.2 MPa, whereas the maximum normal stress is approximately 5.6 MPa. Hence, the normal stress values are approximately 4 to 5 times the shear stress values.

### 4.2 Evolution of stresses along the resistant section

Fig. 5 displays the evolution of normal stress  $\sigma_{xx}$  at some nodes located on the resistant ligament, with the imposed displacement (up to 0.3 mm) on the left side, and the repartition of the same normal stress along the resistant ligament at various imposed displacement values on the right side. The nodes are numbered in increasing order beginning from the crack tip (node 1) to the upper surface of the specimen (node 20). The calculations were run at 20, 150, 300 and 500°C. The sign of the stress and the stress evolution depend on the distance of each node from the crack tip. General observations show that the nodes near the crack tip experience the highest stresses, essentially of the tensile type, whereas those far from the crack tip and near the specimen top face experience essentially compressive stresses. The nodes located in the

intermediate zones experience little tensile stress or tensile stress followed by compressive stress evolving in a sinusoidal form. Whatever the temperature considered, the maximum stress occurs at the notch tip that is a singular point where stresses are localised. On the other hand, the evolution of the stresses along the resistant ligament is similar for all test temperatures. This means that the tension zone near the crack tip moves upstream with increasing applied load and, of course, with the progression of the crack tip. These figures also show that the extent of the tension zone ahead of the crack tip increases with increasing imposed displacement. As expected, the maximum values of the stresses occur at 300°C, which is consistent with the experimental results [1].



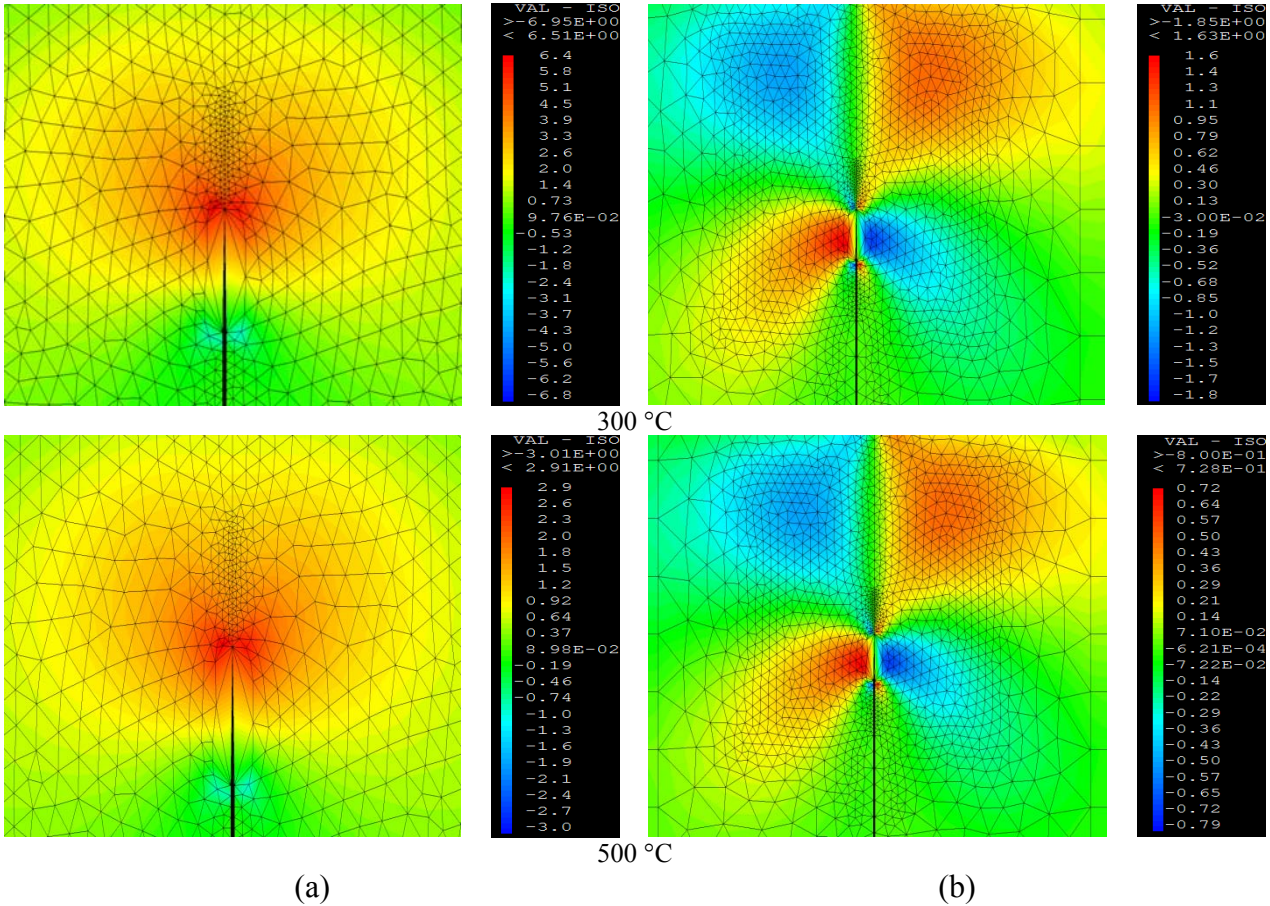
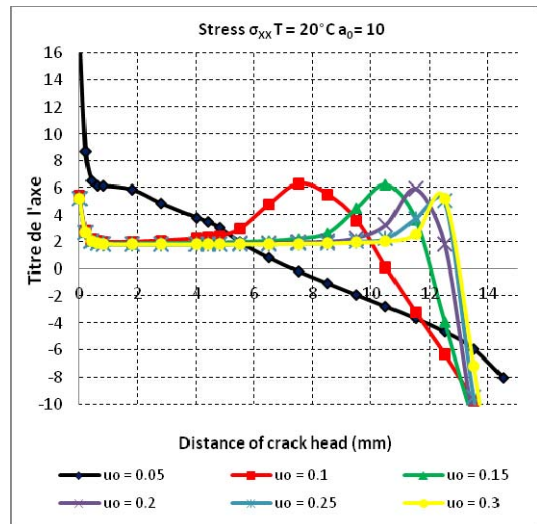
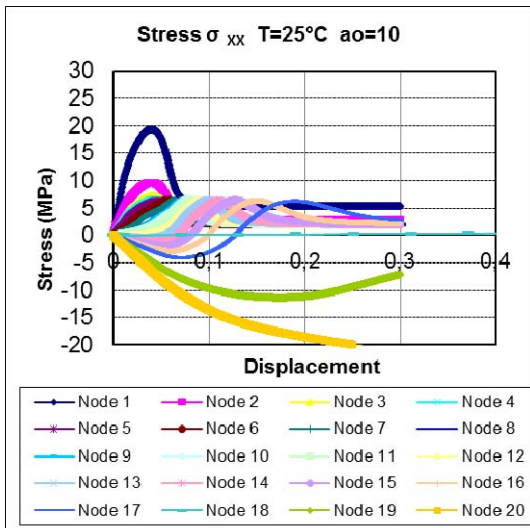
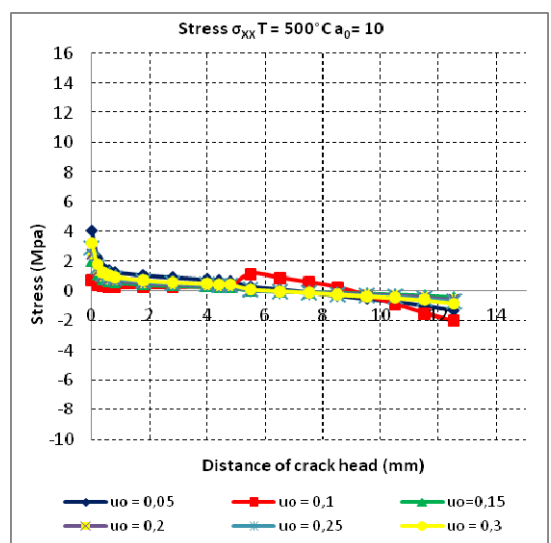
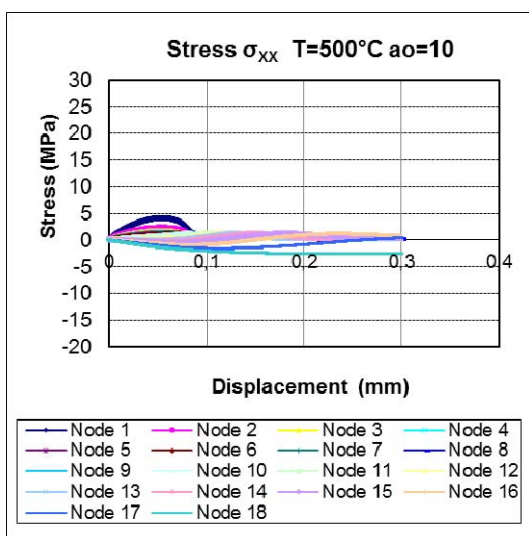
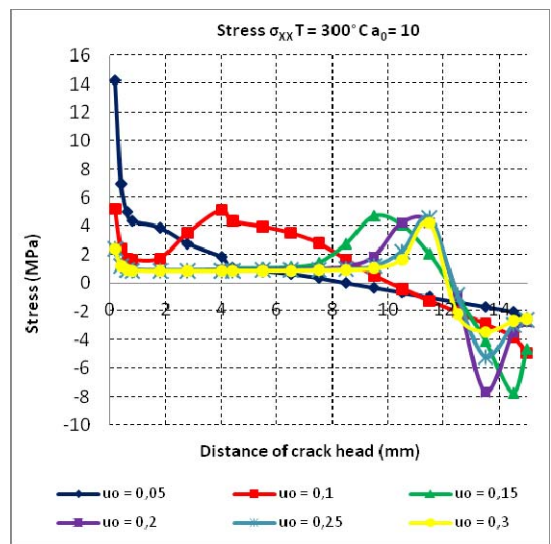
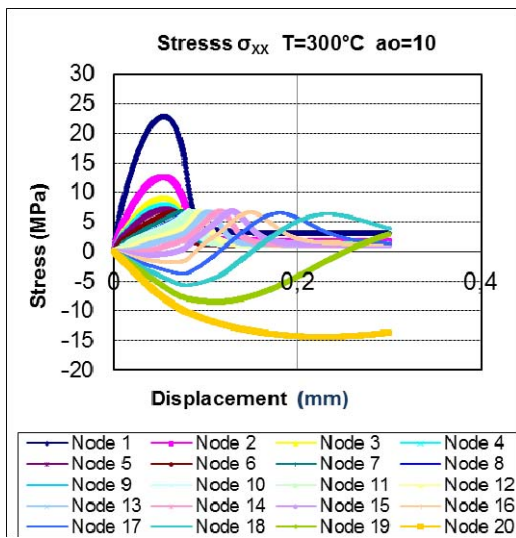
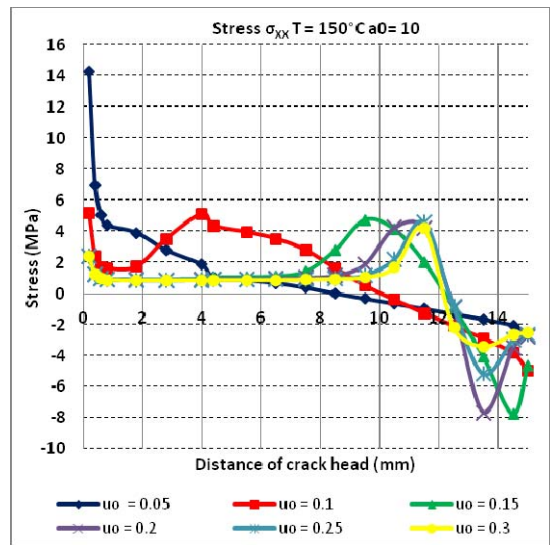
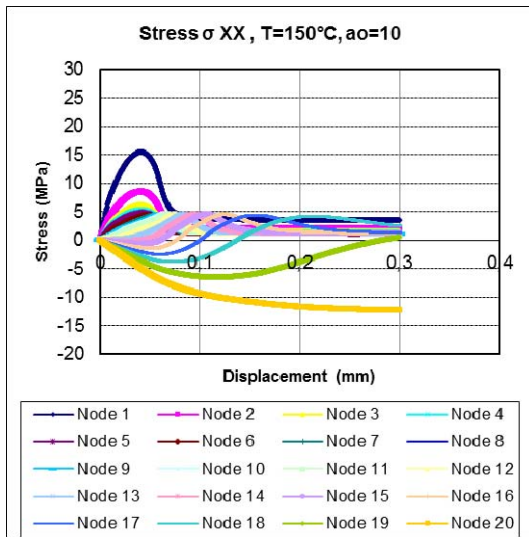


Fig. 4. Distribution of normal stress  $\sigma_{xx}$  (a) and shear stress  $\sigma_{xy}$  (b) around the notch plane at various temperatures (20, 150, 300 and 500°C).

The plots on the right side of Fig. 5 show the evolution of stress as a function of loading at points (nodes) defined previously. It should be noted that the closer the crack tip is, the higher the maximum stress that occurs during loading is. This is true for both the  $\sigma_{XX}$  and  $\sigma_{YY}$  stresses. A few nodes away from the crack tip, the

maximum stress decreases sharply to a level that tends to remain constant for both  $\sigma_{XX}$  and  $\sigma_{YY}$ . Presumably, this limit is characteristic of the tensile strength of the material and is, for  $\sigma_{XX}$ , for example, 6 MPa at 25°C, 5 MPa at 150°C, 7 MPa 300°C and 2 MPa at 500°C (see Fig. 5-b).





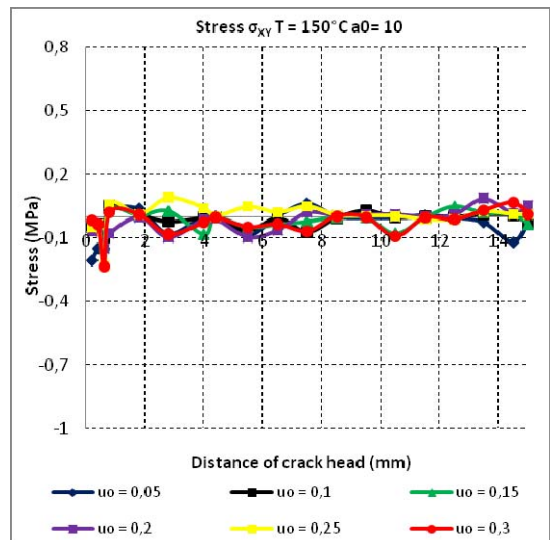
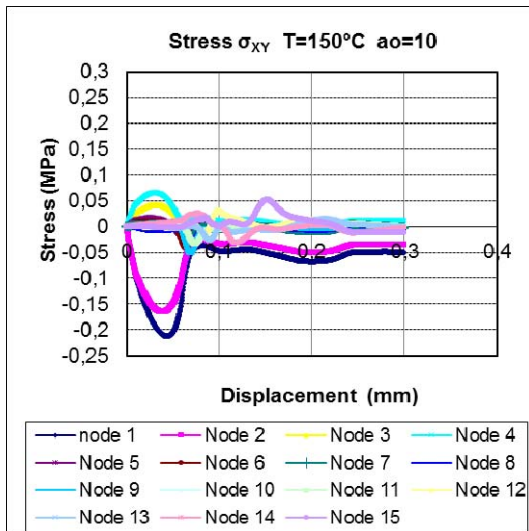
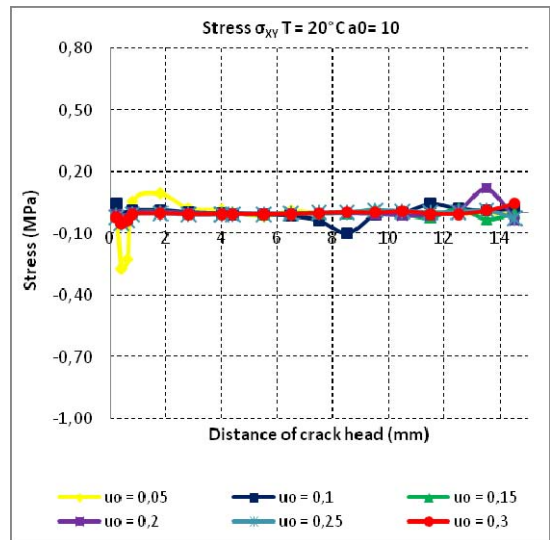
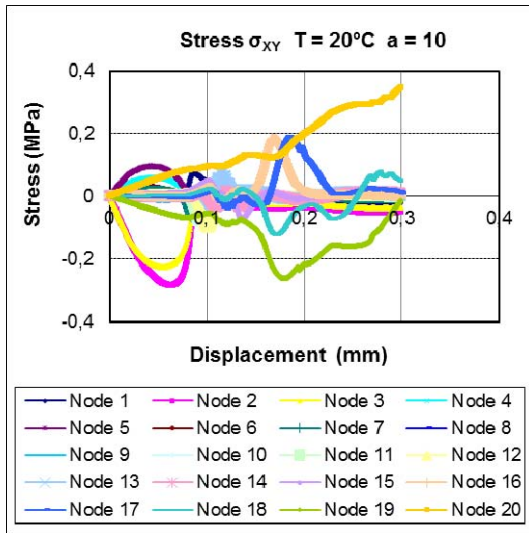
(a)

(b)

**Fig. 5.** Evolution of the normal stress  $\sigma_{xx}$  with the imposed displacement at different nodes (a) and with the distance to the crack tip at various imposed displacements (b) at various testing temperatures (20, 150, 300 and 500°C).

As Fig. 6 shows, the evolution of the shear stress  $\sigma_{XY}$  varies in a very irregular manner with increasing loading. However, in terms of magnitude, the stress  $\sigma_{XY}$  is negligible compared to  $\sigma_{XX}$  and  $\sigma_{YY}$ . This reflects the mode I fracture behaviour simulated properly by the bending test. The maximum shear stresses are observed

near the crack tip and in the tension-to-compression transition zone. Finally, with respect to the effect of temperature on the evolution of these stresses, it appears that the temperature has an effect on their magnitudes but little effect or no effect on their mode of evolution.



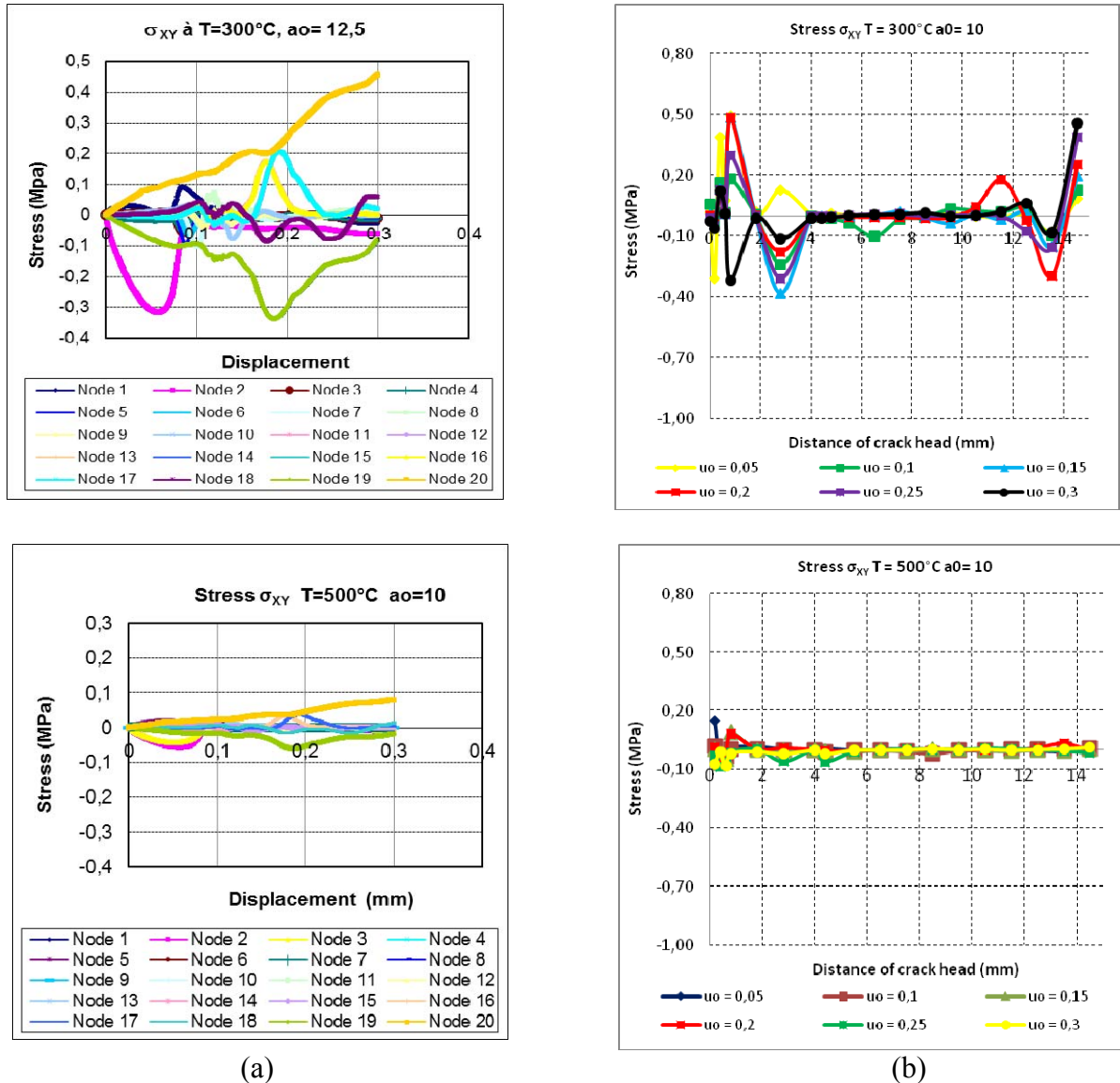


**Fig. 6.** Evolution of the shear stress  $\sigma_{XY}$  with the imposed displacement at different nodes (a) and with distance to the crack tip at various imposed displacements (b) for various heating temperatures (20, 150, 300 and 500°C).

### 4.3 Damage distribution

Fig. 7 displays maps of damage at various loading steps determined from calculations run at various test temperatures. During the calculations, a total displacement of 0.3 mm was applied in 600 linear increments. Hence, during a load step, a displacement of 0.3 / 600 mm was then applied. Fig. 7 shows columns for the test temperatures (25, 150, 300 and 500°C) and rows for the computation steps (i.e., j = 50, 200, 400, 600) corresponding to some loading levels. The calculations were made for a notch length of 10 mm.

As Fig. 7 shows, damage is initiated, as expected, at the notch tip of the specimen and

then spreads along the notch plane as the load increases. The size and shape of the damaged area evolve until the area reaches the size and shape corresponding to a load level of approximately 50% of the maximum load. The damaged area has either an infinite or eight-sided shape at small loads and tends to take the shape of inverted heart at large loads. The part of the damaged area with high-intensity damage is the one shown in red in each of the plots in Fig. 7. The plots also show that the shape of the damaged area and that of the fully damaged part are perfectly symmetrical about the plane of the notch, which means that the crack will propagate approximately in the plane of the notch. Experimental observations showed that the path

followed by the macro-crack after the failure of the specimen was located in the damage zone, indicating that the experimental results are in agreement with the numerical simulation results.

## 5. CONCLUSIONS

- The Mazars model was employed successfully to assess the stresses and damage fields in notched beams of high-performance concrete during isothermal three-point bending testing at various testing temperatures.
- The stress distribution around the notch plane in a three-point bending test of a notched beam is complex and differs notably from that of an unnotched beam. Normal tensile stresses of significant magnitude occur in the x and y directions, whereas shear stresses are negligible. This finding is consistent with the mode I fracture behaviour that this test is intended to simulate.
- The singularity of the tip of the notch generates a stress concentration that induces high normal tensile stresses in the vicinity of the notch tip. These stresses decrease very quickly to realistic values.
- The damage fields that are concentrated in the notch plane are realistic, due to the non-local approach of the Mazars model and are consistent with increasing loading.

## REFERENCES

- [1] Djaknoun, S., Ouedraogo, E., Ahmed Benyahia, A. 2012. Characterisation of the behaviour of high performance mortar subjected to high temperatures. *Construction and Building Materials* 28 (2012) 176-186.
- [2] Mazars, J., 1984. Application de la mécanique de l'endommagement au comportement non linéaire et à la rupture du béton de structure, *Thèse de Doctorat d'Etat*, Université Paris VI, 283 p.
- [3] Mazars, J., Pijaudier-Cabot, G., 1989. Continuum damage theory - application to concrete. *Journal of Engineering Mechanics*, Vol. 115, p 345-365.
- [4] Roosefid, M., 2006. Etude du Comportement Thermomécanique de deux Bétons Réfractaires silico-alumineux: Application à une poche d'aciérie, *PhD Thesis*, Institut National Polytechnique de Grenoble, 2006, France, 272 p.

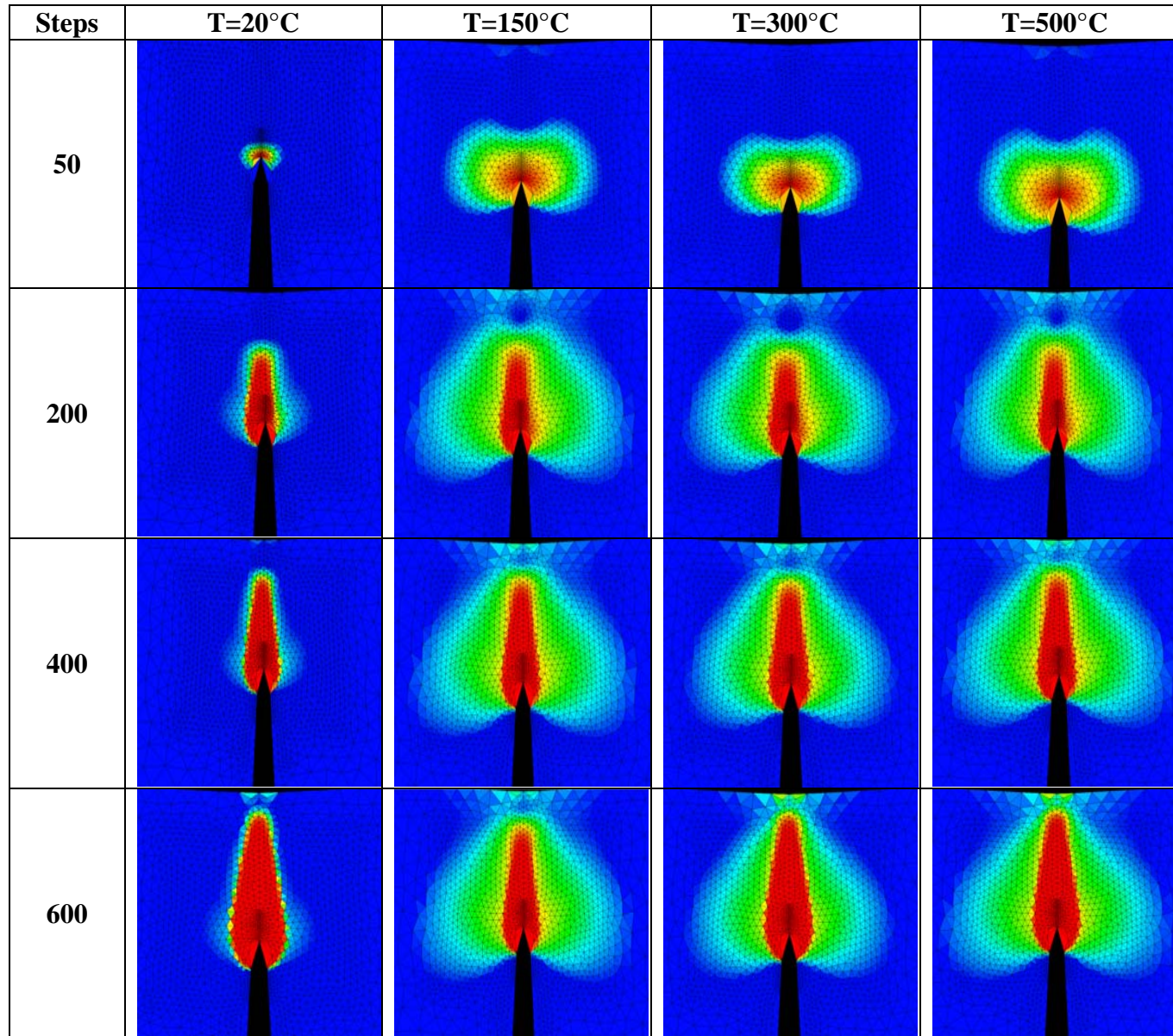


Fig. 7. Distribution of the modelled damage around the notch plane at various loading steps and testing temperatures.